Electric Power Systems Research 152 (2017) 237–248

Contents lists available at ScienceDirect

Electric Power Systems Research

journal homepage: www.elsevier.com/locate/epsr

New modeling framework considering economy, uncertainty, and security for estimating the dynamic interchange capability of multi-microgrids

Fei Xiao*, Qian Ai

Department of Electrical Engineering, Shanghai Jiao Tong University, Shanghai 200240, People's Republic of China

ARTICLE INFO

Article history:
Received 4 January 2017
Received in revised form 16 May 2017
Accepted 3 July 2017

Keywords:
Modeling framework
Dynamic interchange adjustment
Multi-microgrids
Situation awareness
Point estimation method
Second-order conic programming

ABSTRACT

The increasing integration of distributed generation introduces severe challenges to the secure and economical operation of multi-microgrids (MMGs). Therefore, an accurate and timely estimation of secure ranges for dynamic interchange adjustments is necessary for microgrid operators. This study develops a new modeling framework for estimating the interchange capability between MMGs and a distribution network (DN) to increase the situation awareness of the microgrid operator. This framework contains a two models, namely, (1) the proposed prediction model, which considers the economical operation, the robustness of power interchange, and the uncertainty of renewable resources on a microgrid level to obtain the operation states and predicted interchange capabilities, and (2) the correction model, which determines the available interchange capabilities (AICs) while considering the effect of security constraints and spinning reserve on the DN level. AICs ensure the control flexibility and security of microgrids. The approach based on model predictive control is used in this framework to optimize the system operation on the microgrid and DN levels. The point estimation method and second-order conic programming are used to solve the two-level model to guarantee a globally optimal solution and improved computational efficiency. Finally, a distribution system with multiple microgrids is applied to prove the effectiveness of the proposed framework.

1. Introduction

Technological advancements, environmental policies, and energy market deregulation have spurred the deployment of distributed generators (DGs), small renewable installations, and large distributed energy storage systems. Traditional paradigms, which rely on centralized power generation and are distributed through medium-voltage and low-voltage networks, have been adapted to incorporate aggregated systems of DGs (i.e., microgrids) [1]. Coupled with the increasing importance of the Energy Internet, microgrid is one of the fundamental units that provide the same power as the grid with the potential to improve its reliability, power quality, and environmental impact through controls and the coproduction of heating and cooling [2]. The full exploitation of multi-microgrids (MMGs), which involves the design of a new control architecture and the development of novel management tools, has attracted research attention in recent years [3–7].

The dynamic adjustment of interchange flow between adjacent microgrids allows microgrid operators to utilize available internal and external flexible generation resources and available transfer capability (ATC) and provide market participants with cost-saving opportunities in both regions efficiently. In Ref. [5], a centralized multi-objective optimization algorithm was proposed to coordinate MMGs optimally based on a distribution-interline power flow controller. An optimal control algorithm was presented in Ref. [6] for the management of grid-connected MMGs with the Monte Carlo (MC) method. This algorithm finds the optimal operating points of each dependent system in an active distribution grid. Meanwhile, Ref. [7] proposed a decentralized optimal power flow algorithm to coordinate the MMGs and improve the overall performance of a distribution network (DN).

From the development trends of renewable energy and energy marketization, future active distribution grids may include numerous microgrids that work as independent systems with different rules, constraints, and objectives (e.g., reliability maximization, cost minimization, and emission minimization) [5]. Every microgrid operator seeks to manage the amount of power exchange dynamically rather than implement power transactions with no control on

* Corresponding author.
E-mail address: xiaofeisjtu@163.com (F. Xiao).

http://dx.doi.org/10.1016/j.epsr.2017.07.001
0378-7796/

Nomenclature

Symbols, abbreviations, and acronyms

min, max	Minimum and maximum
dch, ch	Discharge and charge
MGCC	Microgrid control center
DNCC	Distribution network control center
PIC	Predicted interchange capability
DPICP	Dynamic power interchange capability prediction
DPICC	Dynamic power interchange capability correction
MG	Microgrid
DG	Distributed generator
PV	Photovoltaic
WT	Wind turbine
MT	Microturbine
DE	Diesel engine
ESD	Energy storage device
BESS	Battery energy storage system
SOC	State of charge

Variables and parameters of the microgrid model

$P_{Mi}^{j,t}$, $P_{Di}^{j,t}$ Power production of the ith MT and the ith DE at hour t in the jth microgrid

$P_{W}^{j,t}$, $P_{V}^{j,t}$ Power production of the WT and PV at hour t in the jth microgrid

$P_{ULi}^{j,t}$, $P_{lLi}^{j,t}$ Power consumption of the ith uninterruptible load and the ith interruptible load at hour t in the jth microgrid

$P_{MTL}^{j,t}$, $H_{MTL}^{j,t}$ Power and heat transmission from cooperative microgrids to the jth microgrid at hour t

$P_{PCC}^{j,t,dn}$, $P_{PCC}^{j,t,up}$ Minimum and maximum power interchange capabilities between the jth microgrid and DN at hour t

$P_{PCC}^{j,t}$ Power transaction at hour t, $P_{PCC}^{j,t} < 0$ if the jth microgrid purchases power from the DN and $P_{PCC}^{j,t} > 0$ if the jth microgrid sells power

$P_{Si}^{j,t}$ Power production of the ith ESD at hour t in the jth microgrid

$W_{Si}^{j,t}$ Stored energy inside the ith ESD at hour t in the jth microgrid

$P_{DGi}^{j,t}$ Power production of the ith DG at hour t in the jth microgrid

$H_{L}^{j,t}$ Heat demand in the jth microgrid at hour t

UR_{Mi}, DR_{Mi} Ramp-up/down rates of the ith MT

UR_{Di}, DR_{Di} Ramp-up/down rates of the ith DE

N_M Number of cooperative microgrids

N_T, N_D, N_S, N_I, N_U Numbers of MT, DE, and ESD units and interruptible and uninterruptible loads in the jth microgrid

Variables and parameters of the distribution network model

$\bar{P}_{PCCi}^{t,dn}$, $\bar{P}_{PCCi}^{t,up}$ Minimum and maximum predicted interchange capabilities between the microgrid and DN at the ith bus and hour t

$\hat{P}_{PCCi}^{t,dn}$, $\hat{P}_{PCCi}^{t,up}$ Minimum and maximum available interchange capabilities between the microgrid and DN at the ith bus and hour t

P_{Li}^{t}, Q_{Li}^{t} Active/reactive powers of the ith bus at hour t

P_{Gi}^{t}, Q_{Gi}^{t} Active/reactive power productions of the slack bus at the ith bus and hour t

P_{Bi}^{t}, Q_{Bi}^{t} Active/reactive power productions of the BESS at the ith bus and hour t

E_{Bi}^{t} Stored energy inside the BESS at the ith bus and hour t

Q_{PCCi}^{t} Reactive power production of the microgrid at the ith bus and hour t

$r_{Gi}^{t,dn}$, $r_{Gi}^{t,up}$ Down/up spinning reserve provisions of the slack bus at the ith bus and hour t

$r_{Bi}^{t,dn}$, $r_{Bi}^{t,up}$ Down/up spinning reserve provisions of the BESS at the ith bus and hour t

V_{i}^{t} Voltage of the ith bus at hour t

δ_{ij}^{t} Voltage phasor difference between the ith and jth buses at hour t

g_{ij}, b_{ij} Conductance and susceptance between the ith and jth buses

N_{DN}, N_G, N_B Numbers of buses, grid-connected microgrids, and BESS in the DN

its tie-line power. Thus, microgrid operators must have real-time knowledge of the secure range for potential interchange adjustments to accomplish the objective of each independent microgrid.

Methods for determining the secure interchange adjustment range include security region methods [8–10] and various advanced nonlinear methods, such as direct methods [11], continuation methods [12–14], nonlinear optimization approaches [15,16], and distributed computation frameworks [17,18]. The majority of these methods are applied to ATC estimation for independent power systems [9–16], while several calculate the interchange capability between multi-area power systems [8,17,18]. Most of these methods consider only physical system constraints (e.g., power line transmission capacity and voltage magnitude) or stability constraints (e.g., limit-induced and saddle-node bifurcations) while preventing the current or near-future system operation situation. Furthermore, a single case study [11–15] cannot cover all operational scenarios even under maximum load generation. Specifically, a single case study for a complicated system, such as MMGs, is highly likely to be significantly different from actual system operating conditions. Thus, the analysis result corresponds to neither an economical nor a secure system operation.

This study develops a new modeling framework that consists of models for dynamic power interchange capability prediction and correction (DPICP and DPICC, respectively) for estimating the secure interchange adjustment range between MMGs and DNs to address the problems mentioned. In the DPICP model, each microgrid operator solves a stochastic multi-objective dispatch problem with a look-ahead period for obtaining the possible economical dispatch points and predicting the upward/downward ramping capability of MMGs. The following uncertainties are dominant in this stochastic problem: (1) heat and electricity load demands and (2) photovoltaic (PV) and wind turbine (WT) power forecast errors. Furthermore, the upward/downward ramping capabilities of controllable units, including microturbine (MT) and diesel engine (DE), are considered in this model. The DPICP model is suitable for calculating the predicted interchange capabilities (PICs) from the perspective of MMG operators who must execute the trade-off between operation cost and control robustness. However, the influence of the exchanging power of MMGs on the security of the DN cannot be overlooked. Therefore, DPICC model-based corrective control measures must be implemented to avoid contingencies on the DN level.

The major contributions of this study are as follows. (1) A new modeling framework based on the model predictive control (MPC) approach is designed for estimating a secure range for dynamic interchange adjustments between MMGs and the DN. The available interchange capabilities (AICs) can still be obtained under this framework should some microgrids isolate themselves from

the grid because of contingency. (2) The multi-objective function adopted in the DPICP model achieves the cooperative operation of the combined heat and power (CHP)-based MMGs while considering the operation cost and the power interchange robustness. (3) A new index is proposed to evaluate the robustness of power interchange. (4) The results obtained by the proposed model can be used to assist independent microgrids in participating autonomously in the ramp market [19] and the demand response market. (5) High accuracy and computational speed are achieved with the proposed method, which combines Hong's point estimation method (PEM) and the second-order conic programming (SOCP) algorithm.

The remainder of this paper is organized as follows. Section 2 describes the proposed framework for the estimation of dynamic interchange capability. Sections 3 and 4 present the DPICP and DPICC models and their solutions, respectively. Section 5 presents the case studies and the analysis of the results. Finally, Section 6 presents the conclusions.

2. Modeling framework of dynamic power interchange estimation

2.1. General framework of the proposed estimation process

The modeling of energy systems has been investigated for several decades. Consequently, realistic and complex modeling tools have been developed to solve various problems in system operations. The combination of different models in one framework maximizes the strengths of these models and captures more of an energy system's dimensions without the large computational requirements of a single large modeling tool [20]. Fig. 1 shows the proposed framework using the DPICP and DPICC models in an iterative cycle for estimating the power interchange capability while ensuring operation security on the microgrid and DN levels.

The DPICP model has two objectives: (1) minimization of operation costs for cooperative MMGs and (2) maximization of power interchange robustness. Each microgrid control center (MGCC) determines the PICs using the fuzzy satisfying method and sends them to the distribution network control center (DNCC). The upload process is incorporated to consider the possible near-future operation situation of MMGs and the disconnection/connection conditions of microgrids. Then, the PICs, including power transactions, are reported to the DNCC, which determines the AICs for microgrid operators based on the DPICC model and the information from the DN level to maintain the security of the entire distribution system. Such information includes the uploaded PICs, the DN operation cost, and the spinning reserve demand. As shown in Fig. 1, the up and down spinning reserves are supported by the battery energy storage system (BESS) and the upstream network in the DPICC model.

2.2. MPC-based approach for MGCC and DNCC scheduling

A MPC-based approach is proposed for each MGCC and DNCC to schedule their available resources and determine the PICs and AICs. In this approach, the forecasts of loads and renewable resources derived from historical data are utilized to obtain the possible optimal operation points of MMGs and DNs. The prediction and correction procedures are repeated at each time slot to ensure that appropriate operational measures are taken in response to unforeseen changes. This MPC-based approach and the timeline for the sequential coordination of MGCC and DNCC are depicted in Fig. 2.

According to the proposed MPC-based scheme, MGCC and DNCC first solve the DPICP and DPICC models, respectively, over the next T time slots based on the predicted values. Subsequently, microgrid operators re-dispatch tie-line power based on the AICs indicated by the DNCC for time slot $k+1$. This power interchange estimation routine is repeated in the succeeding time slots to determine the operational measures in time slots $k+2$, $k+3$, and so on. AICs are provided to microgrid operators for reference only, and the actual re-dispatch of tie-line power that interchanges with the DN is determined and controlled by independent microgrids.

3. Problem formulation

3.1. Formulation of the proposed DPICP model

The DPICP model aims to minimize the MMG operation cost and maximize the power interchange robustness, as formulated in Eq. (1). According to the flexibility of the power system, the power interchange robustness is at the optimum level when the upward and downward ramping capabilities are equal [21]. Ramping capabilities in this study are provided by the MTs, DEs, and interruptible loads. To ensure consistency in the operation cost function, the index of the power interchange robustness is designed as follows.

3.1.1. Objective functions of the DPICP model

$$\min F_1(\boldsymbol{X}_1) = W_1 J_{1.pu} + W_2 J_{2.pu} \tag{1}$$

where

$$J_1 = \sum_{t=k+1}^{t=k+T} \sum_{j=1}^{N_M} (C_{MT}^{j,t} + C_{DE}^{j,t} + C_{MO}^{j,t} + C_{I}^{j,t} - C_{PCC}^{j,t})$$

$$J_2 = \sum_{t=k+1}^{t=k+T} \left(\frac{\eta^{t,up} - \eta^{t,dn}}{\eta^{t,up} + \eta^{t,dn}}\right)^2$$

$$\eta^{t,up} = \sum_{j=1}^{N_M} (P_{PCC}^{j,t,up} - P_{PCC}^{j,t}), \quad \eta^{t,dn} = \sum_{j=1}^{N_M} (P_{PCC}^{j,t} - P_{PCC}^{j,t,dn})$$

$$P_{PCC}^{j,t,up} = P_{PCC}^{j,t} + \sum_{i=1}^{N_T} \min(P_{Mi}^{j,\max} - P_{Mi}^{j,t}, UR_{Mi}) + \sum_{i=1}^{N_D} \min(P_{Di}^{j,\max} - P_{Di}^{j,t}, UR_{Di}) + P_{ILi}^{j,t}$$

$$P_{PCC}^{j,t,dn} = P_{PCC}^{j,t} - \sum_{i=1}^{N_T} \min(P_{Mi}^{j,t} - P_{Mi}^{j,\min}, DR_{Mi}) - \sum_{i=1}^{N_D} \min(P_{Di}^{j,t} - P_{Di}^{j,\min}, DR_{Di})$$

where $\boldsymbol{X}_1 = [\boldsymbol{P_M}, \boldsymbol{P_D}, \boldsymbol{P_S}, \boldsymbol{P_{IL}}, \boldsymbol{P_{PCC}}, \boldsymbol{P_{MTL}}, \boldsymbol{H_{MTL}}]$ is the vector of control variables on the microgrid level, including MT, DE, ESD production, interruptible load, power transaction, and power and heat transmission vectors. Parameters W_1 and W_2 are the weighting factors that adjust the influence of different terms on the multi-objective operation function. $J_{1.pu}^t$ and $J_{2.pu}^t$ denote the normalized objective functions, namely, the operation cost and the power interchange robustness of cooperative MMGs. $\eta^{t,up}$ and $\eta^{t,dn}$ are the upward and downward ramping capabilities of MMGs. Given that the functions in Eq. (1) are not in the same range and dimension, a fuzzy satisfying method is used to calculate the normalized form of the objective functions [22]. Specifically, operation cost J_1 has five components, namely, $C_{MT}^{j,t}$, $C_{DE}^{j,t}$, $C_{MO}^{j,t}$, $C_{I}^{j,t}$, and $C_{PCC}^{j,t}$, that are expressed as follows:

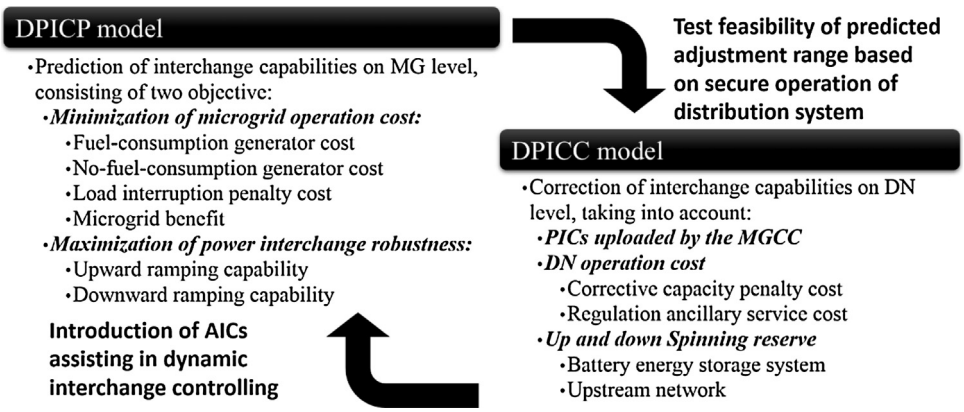

Fig. 1. Proposed modeling framework.

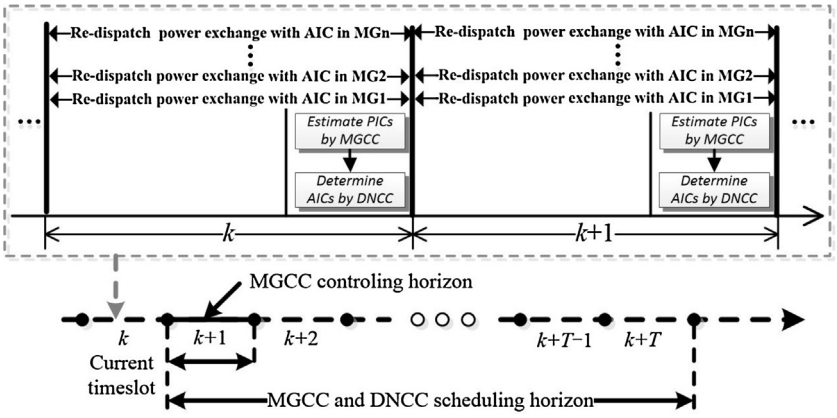

Fig. 2. Timeline for the sequential coordination of MGCC and DNCC in a DN, including coupled microgrids.

Fuel-consumption generator cost [23]:

$$C_{MT}^{j,t} = \sum_{i=1}^{N_T} c_{MT} \frac{P_{Mi}^{j,t}}{\eta_{Mi}} \quad t = k+1, \ldots, k+T; \quad j = 1, \ldots, N_M \tag{2}$$

$$C_{DE}^{j,t} = \sum_{i=1}^{N_D} [a(P_{Di}^{j,t})^2 + bP_{Di}^{j,t} + c] \quad t = k+1, \ldots, k+T; \quad j = 1, \ldots, N_M \tag{3}$$

where c_{MT} and η_{Mi} are the fuel price and the fuel conversion efficiency of MT, respectively. a, b, and c are the coefficients of the DE cost curve.

No-fuel-consumption generator cost:

$$C_{MO}^{j,t} = \sum_{i=1}^{N_S} c_{SB} P_{Si,\mathrm{ch/dch}}^{j,t} + c_{WT} P_W^{j,t} + c_{PV} P_V^{j,t} \quad t = k+1, \ldots, k+T; \quad j = 1, \ldots, N_M \tag{4}$$

where c_{SB}, c_{WT}, and c_{PV} represent the maintenance cost coefficients of ESD, WT, and PV, respectively.

Load interruption penalty cost:

$$C_I^{j,t} = \beta_I \sum_{i=1}^{N_I} (P_{ILi}^{j,t,\ \max} - P_{ILi}^{j,t}) \quad t = k+1, \ldots, k+T; \quad j = 1, \ldots, N_M \tag{5}$$

where β_I is the interruption cost coefficient.

Microgrid benefits:

$$C_{PCC}^{j,t} = c_P^t P_{PCC}^{j,t} \quad t = k+1, \ldots, k+T; \quad j = 1, \ldots, N_M \tag{6}$$

where c_P^t denotes the market price. This study is based on a net metering approach in which the price of buying and selling energy is the same for all microgrids.

3.1.2. Constraints of the DPICP model

Power balance:

$$\sum_{i=1}^{N_T} P_{Mi}^{j,t} + \sum_{i=1}^{N_D} P_{Di}^{j,t} + \sum_{i=1}^{N_S} P_{Si}^{j,t} + P_V^{j,t} + P_W^{j,t} + P_{MTL}^{j,t} = P_{PCC}^{j,t} + \sum_{i=1}^{N_U} P_{ULi}^{j,t} + \sum_{i=1}^{N_I} P_{ILi}^{j,t} \quad t = k+1, \ldots, k+T; \quad j = 1, \ldots, N_M \tag{7}$$

Spinning reserve requirements [23]:

$$\sum_{i=1}^{N_T} \min(P_{Mi}^{j,\max} - P_{Mi}^{j,t}, UR_{Mi}) + \sum_{i=1}^{N_D} \min(P_{Di}^{j,\max} - P_{Di}^{j,t}, UR_{Di}) + \sum_{i=1}^{N_S} \eta_{SDi}(W_{Si}^{j,t} - W_{Si}^{j,\min}) \geq \kappa_{DG} P_{DG}^{j,\max} + \kappa_V P_V^{j,t} + \kappa_W P_W^{j,\max} + \kappa_L \sum_{i=1}^{N_U} P_{ULi}^{j,t} \quad t = k+1, \ldots, k+T; \quad j = 1, \ldots, N_M \tag{8}$$

where κ_{DG}, κ_V, κ_W, and κ_L are the factors of the microgrid spinning reserve.

Heat balance:

$$H_L^{j,t} = k_{Mi}\sum_{i=1}^{N_T} P_{Mi}^{j,t} + H_{MTL}^{j,t} \quad t = k+1,\ldots,k+T;\quad j = 1,\ldots,N_M \tag{9}$$

where k_{Mi} is the heat-to-power ratio of the ith MT [24].

Tie-line transfer capability limits within cooperative microgrids:

$$P_{MTL}^{j,\min} \le P_{MTL}^{j,t} \le P_{MTL}^{j,\max} \quad t = k+1,\ldots,k+T;\quad j = 1,\ldots,N_M \tag{10}$$

$$H_{MTL}^{j,\min} \le H_{MTL}^{j,t} \le H_{MTL}^{j,\max} \quad t = k+1,\ldots,k+T;\quad j = 1,\ldots,N_M \tag{11}$$

$$\sum_{j=1}^{N_M} P_{MTL}^{j,t} = \sum_{j=1}^{N_M} H_{MTL}^{j,t} = 0 \quad t = k+1,\ldots,k+T;\quad j = 1,\ldots,N_M \tag{12}$$

Active power limits of DGs [25]:

$$P_{DGi}^{j,t,\min} \le P_{DGi}^{j,t} \le P_{DGi}^{j,t,\max} \quad t = k+1,\ldots,k+T;\quad j = 1,\ldots,N_M \tag{13}$$

$$\begin{aligned} &P_{DGi}^{j,t} - P_{DGi}^{j,t-1} \le UR_{DGi} \\ &P_{DGi}^{j,t-1} - P_{DGi}^{j,t} \le DR_{DGi} \end{aligned} \quad t = k+1,\ldots,k+T;\quad j = 1,\ldots,N_M \tag{14}$$

Power interchange capability limits:

$$P_{PCC}^{j,\min} \le P_{PCC}^{j,t} \le P_{PCC}^{j,\max} \quad t = k+1,\ldots,k+T;\quad j = 1,\ldots,N_M \tag{15}$$

Energy storage limits related to ESD [25]:

$$\begin{aligned} &W_{Si}^{j,t} = W_{Si}^{j,t-1} + \eta_{SCi}P_{Si,\mathrm{ch}}^{j,t}\Delta t - \frac{1}{\eta_{SDi}}P_{Si,\mathrm{dch}}^{j,t}\Delta t \\ &t = k+1,\ldots,k+T;\quad j = 1,\ldots,N_M;\qquad \Delta t = 1h \end{aligned} \tag{16}$$

$$W_{Si}^{j,\min} \le W_{Si}^{j,t} \le W_{Si}^{j,\max} \quad t = k+1,\ldots,k+T;\quad j = 1,\ldots,N_M \tag{17}$$

$$-P_{Si,\mathrm{ch}}^{j,\max} \le P_{Si}^{j,t} \le P_{Si,\mathrm{dch}}^{j,\max} \quad t = k+1,\ldots,k+T;\quad j = 1,\ldots,N_M \tag{18}$$

where η_{SCi} and η_{SDi} are the efficiencies of the ith ESD during the charge and discharge processes.

Limits of load interruption [25]:

$$0 \le P_{ILi}^{j,t} \le P_{ILi}^{j,t,\max} \quad t = k+1,\ldots,k+T;\quad j = 1,\ldots,N_M \tag{19}$$

3.1.3. Uncertainty characterization of the DPICP model

The uncertainties of PV, WT power, and load demand forecasting error affect the microgrid operation. Therefore, the corresponding probabilistic models should be constructed on the microgrid level. The probability density functions (PDFs) of the PV, WT power, and load demand forecast error in each month are obtained from historical data, which include the stochastic time series of PV and the WT generation over a one-year period [26,27].

According to Ref. [26], the forecast errors of random variables have their own PDFs with mean values that are close to 0 and their standard deviation (STD) is related to their nominal power. Moreover, the STD of the random variables is used to indicate their dispersion [28,29]. Assuming that the dispersion of variables is normal, approximately 99.73% of the variables are within three STDs ($\mu \pm 3\sigma$). Thus, three STDs ($\pm 3\sigma$) are adopted to the PIC estimation in Eq. (20):

$$\begin{aligned} &\tilde{P}_{PCCi}^{t,up} = \min(E(P_{PCC}^{j,t,up}) + 3\sigma(P_{PCC}^{j,t,up}), P_{PCC}^{j,\max}) \\ &\tilde{P}_{PCCi}^{t,dn} = \max(E(P_{PCC}^{j,t,dn}) - 3\sigma(P_{PCC}^{j,t,dn}), P_{PCC}^{j,\min}) \\ &\quad t = k+1,\ldots,k+T;\quad j = 1,\ldots,N_M \end{aligned} \tag{20}$$

where functions $E(\cdot)$ and $\sigma(\cdot)$ are used to calculate the expectation and the STD of the variables, respectively. The specific procedures for solving this stochastic problem are illustrated in Section 4.

3.2. Formulation of the proposed DPICC model

The goal of a DN operator is to coordinate the spinning reserve while minimizing the sum of DN operation costs, including the corrective capacity penalty and regulation ancillary service costs.

3.2.1. Objective functions of the DPICC model

$$\begin{aligned} &\min F_2(\boldsymbol{X}_2) \\ &= \sum_{t=k+1}^{t=k+T}\left\{\sum_{i=1}^{N_G} c_P\left(|\tilde{P}_{PCCi}^{t,up} - \hat{P}_{PCCi}^{t,up}| + |\tilde{P}_{PCCi}^{t,dn} - \hat{P}_{PCCi}^{t,dn}|\right) + c_R^t P_{Gi}^t\right\} \end{aligned} \tag{21}$$

where $\boldsymbol{X}_2 = [\boldsymbol{P_G}, \boldsymbol{P_B}, \boldsymbol{Q_G}, \boldsymbol{Q_B}, \boldsymbol{Q_{PCC}}]$ is the DN level vector of the control variables, including active power production vectors of the slack bus, BESS and reactive power production vectors of the slack bus, BESS, and microgrids. c_P is the penalty price for correcting the secure range predicted by MMGs. c_R^t is the regulation market price. The lines of most DNs, except those in dense urban areas, are loaded significantly below their thermal capacity [30]. Thus, thermal limits are not considered in the DPICC model. All grid-connected microgrids operate in PQ modes [31].

3.2.2. Constraints of the DPICC model

AC power balance:

$$\begin{aligned} &P_{Gi}^t - P_{Li}^t + P_{Bi}^t + P_{PCCi}^t = \sum_{j=1}^{N_{DN}}\left[g_{ij}(V_i^t)^2 - g_{ij}V_i^tV_j^t\cos\delta_{ij}^t + b_{ij}V_i^tV_j^t\sin\delta_{ij}^t\right] \\ &Q_{Gi}^t - Q_{Li}^t + Q_{Bi}^t + Q_{PCCi}^t = \sum_{j=1}^{N_{DN}}[b_{ij}(V_i^t)^2 - b_{ij}V_i^tV_j^t\cos\delta_{ij}^t - g_{ij}V_i^tV_j^t\sin\delta_{ij}^t] \\ &t = k+1,\ldots,k+T;\quad i = 1,\ldots,N_{DN} \end{aligned} \tag{22}$$

The vector of P_{PCCi}^t is equal to the power transactions solved using the DPICP model.

Active and reactive power limits of the slack bus:

$$\begin{aligned} &P_{Gi}^{\min} \le P_{Gi}^t \le P_{Gi}^{\max} \\ &Q_{Gi}^{\min} \le Q_{Gi}^t \le Q_{Gi}^{\max} \end{aligned} \quad t = k+1,\ldots,k+T \tag{23}$$

Reactive power limits at the point of common coupling between microgrids and DN:

$$Q_{PCCi}^{\min} \le Q_{PCCi}^t \le Q_{PCCi}^{\max} \quad t = k+1,\ldots,k+T \tag{24}$$

Microgrid reactive power production is limited by their interfacing converter sizes.

Bus voltage limits:

$$V_i^{\min} \le V_i^t \le V_i^{\max} \quad t = k+1,\ldots,k+T \tag{25}$$

Energy storage limits related to BESS [32]:

$$\begin{aligned} &-P_{Bi,\mathrm{ch}}^{\max} \le P_{Bi}^t \le P_{Bi,\mathrm{dch}}^{\max} \\ &-Q_{Bi}^{\max} \le Q_{Bi}^t \le Q_{Bi}^{\max} \end{aligned} \quad t = k+1,\ldots,k+T \tag{26}$$

$$(P_{Bi}^t)^2 + (Q_{Bi}^t)^2 \le (S_{Bi}^{\max})^2 \quad t = k+1,\ldots,k+T \tag{27}$$

$$\begin{aligned} &E_{Bi}^t = E_{Bi}^{t-1} + \eta_{BCi}P_{Bi,\mathrm{ch}}^t\Delta t - \frac{1}{\eta_{BDi}}P_{Bi,\mathrm{dch}}^t\Delta t \\ &\quad t = k+1,\ldots,k+T;\quad \Delta t = 1h \end{aligned} \tag{28}$$

$$E_{Bi}^{\min} \le E_{Bi}^t \le E_{Bi}^{\max} \quad t = k+1,\ldots,k+T \tag{29}$$

$$E_{Bi}^{t=k+1} = E_{Bi}^{t=k+T} \tag{30}$$

where η_{BCi} and η_{BDi} are the efficiencies of BESS at the ith bus during the charge and discharge processes. The constraint (26) and

the capability curve of the active and reactive powers of charging/discharging are modeled by Eq. (27).

Spinning reserve provision limits related to the slack bus [32]:

$$r_{Gi}^{t,up} + P_{Gi}^{t} \le P_{Gi}^{\max} \quad \text{and} \quad P_{Gi}^{t} - r_{Gi}^{t,dn} \ge P_{Gi}^{\min} \quad t = k+1, \ldots, k+T \tag{31}$$

$$r_{Gi}^{t,up/dn} \le R_{Gi}^{up/dn,\max} \quad t = k+1, \ldots, k+T \tag{32}$$

where $R_{Gi}^{up/dn,\max}$ is the maximum slack bus contribution for up and down spinning reserves.

Spinning reserve provision limits related to the BESS [32]:

$$r_{Bi}^{t,up} + P_{Bi}^{t} \le P_{Bi,\mathrm{dch}}^{\max} \quad \text{and} \quad r_{Bi}^{t,dn} - P_{Bi}^{t} \le P_{Bi,\mathrm{ch}}^{\max} \quad t = k+1, \ldots, k+T \tag{33}$$

$$E_{Bi}^{t} - \frac{1}{\eta_{BDi}}(r_{Bi}^{t,up} + P_{Bi}^{t})\Delta t \ge E_{Bi}^{\min} \quad t = k+1, \ldots, k+T; \quad \Delta t = 1h \tag{34}$$

$$E_{Bi}^{t} + \eta_{BCi}(r_{Bi}^{t,dn} - P_{Bi}^{t})\Delta t \le E_{Bi}^{\max} \quad t = k+1, \ldots, k+T; \quad \Delta t = 1h \tag{35}$$

The limited reservoir capacity of BESS results in a time-limited reserve provision. Therefore, Eqs. (34) and (35) are considered in this study.

Spinning reserve constraints [32]:

$$\begin{aligned} &\sum_{i=1}^{N_B} r_{Bi}^{t,up} + r_{Gi}^{t,up} \ge \sum_{i=1}^{N_G} \left(P_{PCCi}^{t} - \hat{P}_{PCCi}^{t,dn} \right) + \lambda_R \sum_{i=1}^{N_{DN}} P_{Li}^{t} \\ &\sum_{i=1}^{N_B} r_{Bi}^{t,dn} + r_{Gi}^{t,dn} \ge \sum_{i=1}^{N_G} \left(\hat{P}_{PCCi}^{t,up} - P_{PCCi}^{t} \right) + \lambda_R \sum_{i=1}^{N_{DN}} P_{Li}^{t} \\ &t = k+1, \ldots, k+T \end{aligned} \tag{36}$$

where λ_R is the rate of the spinning reserve requirement related to load demand. The AICs of each microgrid are scheduled based on the proportion of PICs reported by the microgrids [33].

Feasible solution requirements:

$$\tilde{P}_{PCCi}^{t,dn} \le \hat{P}_{PCCi}^{t,dn} \le P_{PCCi}^{t} \le \hat{P}_{PCCi}^{t,up} \le \tilde{P}_{PCCi}^{t,up} \quad t = k+1, \ldots, k+T \tag{37}$$

4. Solution procedure

In the proposed modeling framework, sequence quadratic programming (SQP) and PEM are used to solve the DPICP model. Given the nonconvex results of the DPICC model, the identification of the global optimal solution is a complex process. Thus, SOCP is used to transform the original DPICC model to a convex programming problem.

4.1. Stochastic PIC calculation using the PEM

PEM is an approximation method that directly provides the first few statistical moments of random output based only on a few deterministic optimization calculations. Compared with the MC method, the PEM generally imposes a low computation burden.

Different schemes can be applied in the frame of the PEM. Currently, $2m$, $2m+1$, and $4m+1$ PEM schemes are widely used to solve probabilistic power flow problems [29,34,35]. The $2m+1$ PEM scheme provides the best solution in terms of accuracy and computation effort and is the most efficient scheme for dealing with normal distribution. This study assumes that the behavior of all the input random variables are similar to the normal distribution function [36]. Therefore, this assumption indicates that the $2m+1$ PEM scheme is a suitable tool to cover the uncertainty effect.

PEM focuses on the statistical information provided by the few initial central moments of random variables on s points for each variable, hereby designated as concentrations. The relationship between input and output can be obtained using these points and function F. The sth concentration $(x_{l,s}, w_{l,s})$ of an uncertain variable x_l can be defined as a pair composed of location $x_{l,s}$ and weight $w_{l,s}$. Location $x_{l,s}$ is the sth value of variable x_l at which function F is evaluated. Weight $w_{l,s}$ accounts for the relative importance of this evaluation in the output random variables. The number of random variables is m, and the total number of evaluations of F is $s \times m$ [34]. Specifically, the $2m+1$ PEM scheme considers one more evaluation of function F at the point made up of the mean values of the random variables. Therefore, the total number of F evaluations is $2m+1$. The steps in computing the moments of the output variables can be summarized as follows:

Step 1: Determine the number of random variables m and set $l = 1$.

Step 2: Calculate the skewness and kurtosis of uncertain variable x_l:

$$\lambda_{l,j} = \frac{M_j(x_l)}{(\sigma_{xl})^j} = \frac{E[(x_l - \mu_{xl})^j]}{(\sigma_{xl})^j} \quad j = 3, 4 \tag{38}$$

where μ_{xl} and σ_{xl} are the mean and STD of x_l, respectively.

Step 3: Determine the locations of concentrations $(\xi_{l,1}, \xi_{l,2})$ [34]:

$$\xi_{l,s} = \frac{\lambda_{l,3}}{2} + (-1)^{3-s}\sqrt{\lambda_{l,4} - \frac{3}{4}\lambda_{l,3}^2} \quad s = 1, 2 \tag{39}$$

Step 4: Determine the weights as follows:

$$w_{l,s} = \frac{(-1)^{3-s}}{\xi_{l,s}(\xi_{l,1} - \xi_{l,2})} \quad s = 1, 2 \tag{40}$$

Step 5: Obtain the two estimated locations of uncertain variable x_l:

$$x_{l,s} = \mu_l + \xi_{l,s}\sigma_l \quad s = 1, 2 \tag{41}$$

Step 6: Calculate the deterministic problem for the estimated locations:

$$Z(l, s) = F_1(\mu_{x1}, \mu_{x2}, \ldots, x_{l,s}, \ldots, \mu_{xm}) \quad s = 1, 2 \tag{42}$$

In the proposed stochastic PIC calculation method, the deterministic problem is the procedure for solving the multi-objective operation function in Eq. (1) with the SQP-based method.

Step 7: Update $E(Z)$ and $E(Z^2)$ as follows:

$$E(Z^j) = E(Z^j) + \sum_{s=1}^{2} w_{l,s}(Z(l, s))^j \quad j = 1, 2 \tag{43}$$

Step 8: Repeat Steps 2–7 for $l = l + 1$ until the list of random input variables is exhausted.

Step 9: Evaluate $E(Z)$ and $E(Z^2)$ as follows [34]:

$$E(Z^j) = E(Z^j) + w_0(F_1(\mu_{x1}, \mu_{x2}, \ldots \mu_{xm}))^j \quad j = 1, 2 \tag{44}$$

where:

$$w_0 = 1 - \sum_{l=1}^{m} \frac{1}{(\lambda_{l,4} - \lambda_{l,3}^2)}$$

Step 10: Determine the mean and STD of the output variables.

The aforementioned steps can be applied with the correlated random variables using the rotational transformation method [37].

Table 1
Limits and bids of the DGs in MMGs.

Type	Minimum power (kW)	Maximum power (kW)	Ramp up/down rate (kW)	Bid coefficients
PV1/PV2	0	40	–	c_{PV} = 0.0016 $/(kWh)
WT1/WT2	0	80	–	c_{WT} = 0.0016 $/(kWh)
ESD1/ESD2	−20	20	–	c_{SB} = 0.008 $/(kWh), $\eta_{SCi} = \eta_{SDi}$ = 90%
MT1/MT2	0	40	40	c_{MT} = 0.15 $/(kWh), η_{Mi} = 40%
DE1/DE2	0	30	30	a = 0.012 $/(kW^2 h), b = 0.15 $/(kWh), c = 1.1 $/h

This method transforms the correlated set of input random variables into the uncorrelated set of input random variables on the basis of the eigenvalues and corresponding eigenvectors of the covariance matrix.

4.2. Deterministic AIC calculation using the SOCP

The SOCP approach has been applied in power system studies, such as in optimal power flow and transmission system planning, and the global optimal solution of these models has been numerically confirmed [38,39]. The steps in computing the AICs in the DPICC model are as follows:

Step 1: Define new variables as follows:

$$u_i^t = (V_i^t)^2 \tag{45}$$

$$R_{ij}^t = V_i^t V_j^t \cos\delta_{ij}^t \quad \text{and} \quad T_{ij}^t = V_i^t V_j^t \sin\delta_{ij}^t \tag{46}$$

Step 2: Take the magnitude square of Eq. (46) as follows:

$$(R_{ij}^t)^2 + (T_{ij}^t)^2 = u_i^t u_j^t \tag{47}$$

Step 3: Relax the equality constraints expressed in Eq. (47) as follows:

$$(R_{ij}^t)^2 + (T_{ij}^t)^2 \le u_i^t u_j^t \tag{48}$$

Step 4: Replace Eqs. (22) and (25) based on the new variables as follows:

$$\begin{aligned} P_{Gi}^t + P_{Bi}^t - P_{Li}^t + P_{PCCi}^t &= \sum_{j=1}^{N_{DN}} (g_{ij}u_i^t - g_{ij}R_{ij}^t + b_{ij}T_{ij}^t) \\ Q_{Gi}^t + Q_{Bi}^t - Q_{Li}^t + Q_{PCCi}^t &= \sum_{j=1}^{N_{DN}} (b_{ij}u_i^t - b_{ij}R_{ij}^t - g_{ij}T_{ij}^t) \end{aligned} \tag{49}$$

$$u_i^{\min} \le u_i^t \le u_i^{\max} \tag{50}$$

Step 5: Combine the results of the PICs and determine the AICs using the DPICC model.

Given the convexity of the feasible region of the DPICC model, the global optimal solution can be solved using a standard commercial software. The flowchart for solving the DPICP and DPICC models is illustrated in Fig. 3.

5. Case study and numerical results

The mathematical models described previously re applied to a 33-bus distribution system with MMGs, as shown in Fig. 4. The stochastic analysis of the DPICP model is investigated in Section 5.2. The DPICC model is analyzed in Section 5.3.

5.1. Test system

Case I. Seven grid-connected microgrids with cooperative and noncooperative operations within the test distribution system are shown in Fig. 4. The MMG test case, which is composed of MG1 and MG2, is presented in detail to examine the features of the proposed

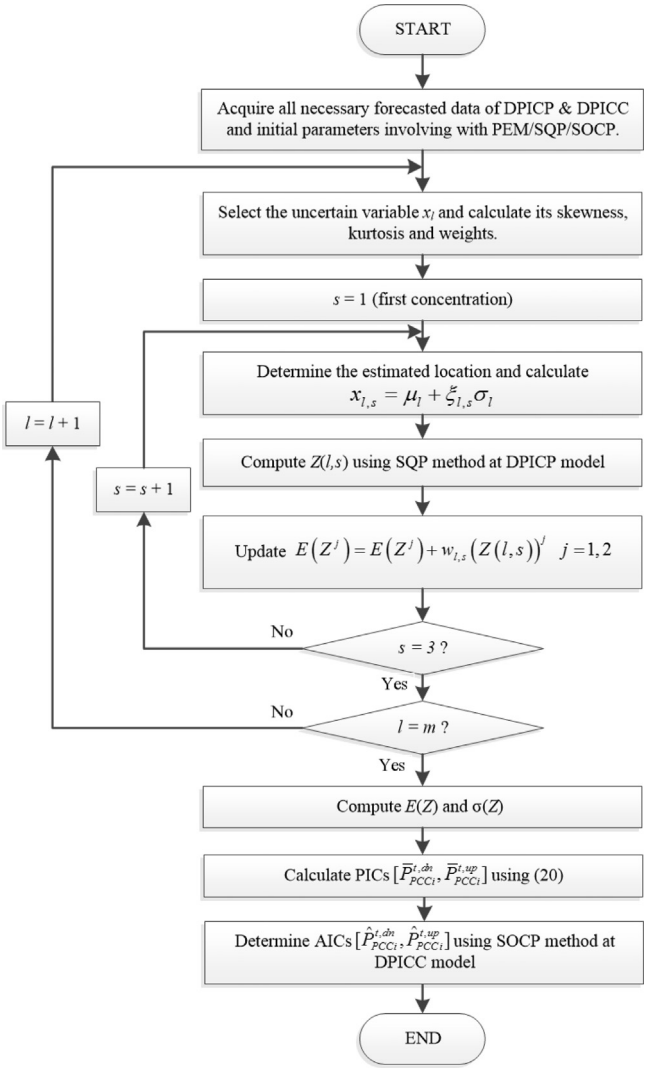

Fig. 3. Flowchart of the implementation of the hybrid method of solving the modeling framework.

Table 2
Limits of the energy storage devices.

Type	Minimum SOC (kWh)	Maximum SOC (kWh)	Initial SOC (kWh)
ESD1	20	200	120
ESD2	20	180	100

DPICP model. This MMG [5] consists of two sets of each of the following: DEs, MTs, ESDs, WTs, and PVs. The tie-line achieves power and heat transmission, which satisfy $P_{MTL}^{1,\max} = P_{MTL}^{2,\max}$ = 20 kW and $H_{MTL}^{1,\max} = H_{MTL}^{2,\max}$ = 20 kW within cooperative microgrids. L1 and L2 are heat loads and L3–L6 are electricity loads, among which L5 and L6 are interruptible. Tables 1 and 2 present the output power limits, ramping up/down limits, and bid coefficients of the DGs in the MMGs.

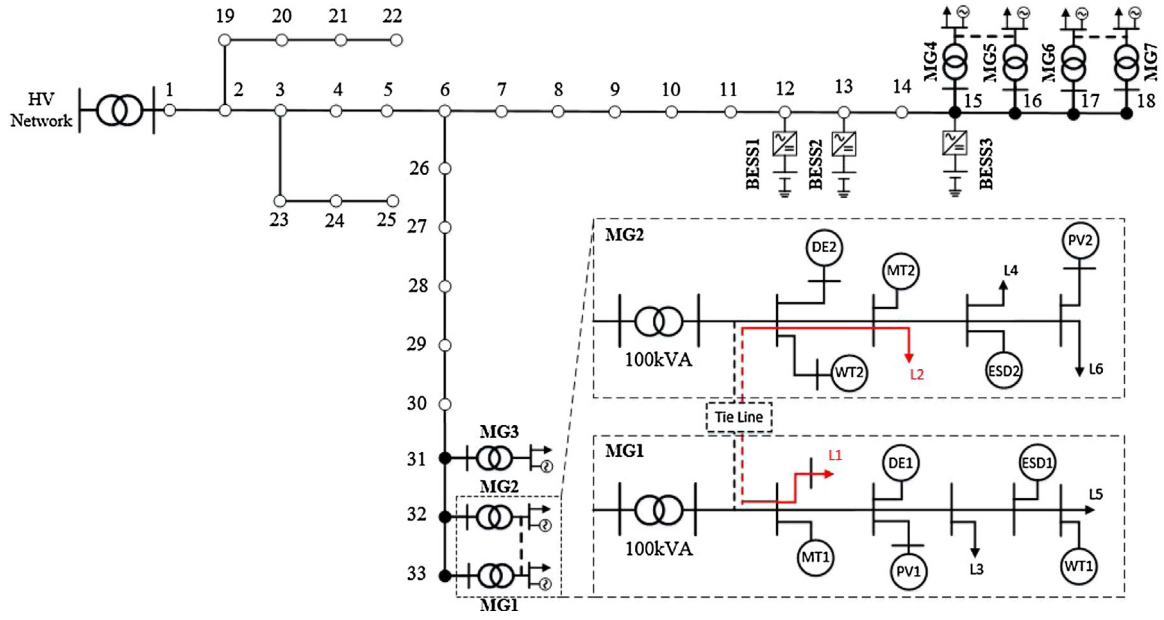

Fig. 4. 33-bus test distribution system with CHP-based MMGs.

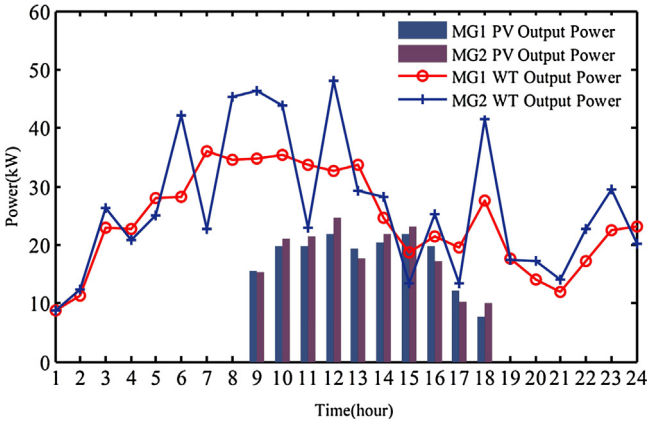

Fig. 5. Forecasted data for PV and WT power.

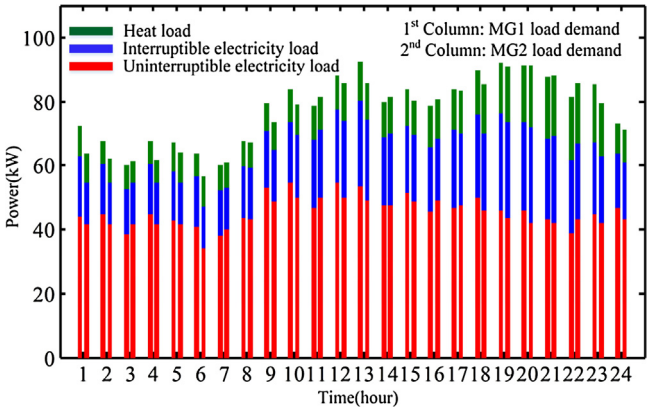

Fig. 6. Forecasted data for load demand.

Case studies are conducted for a sample day in November, and the forecasts for PV, WT power, electricity load, and heat load are shown in Figs. 5 and 6. The STDs of PV, WT power, and load demand are 10%, 15%, and 3% of their forecasted data, respectively [28]. Moreover, spinning reserve parameters κ_{DG}, κ_V, κ_W, and κ_L are set to 0.25, 0.1, 0.15, and 0.03, respectively [23]. The market prices are shown in Table 3 [28].

Table 3
Market prices of upstream power system.

Type of time	Time	Price ($/(kWh))
Peak time	10:00–14:00, 18:00–21:00	0.137
Valley time	00:00–07:00, 23:00–24:00	0.028
Flat time	The rest	0.081

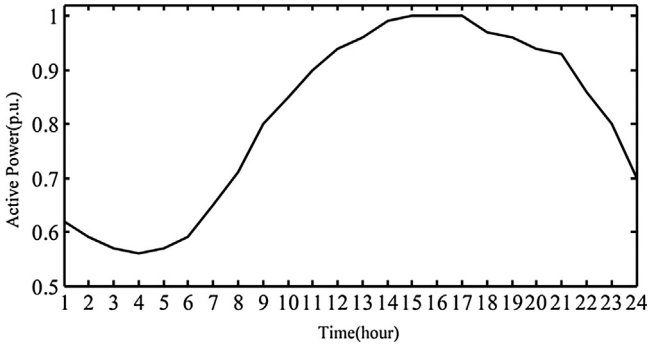

Fig. 7. Daily load curve from the CAISO.

Case II. The 33-bus test system has 32 branches, with Bus 1 as the slack bus. Details of the 33-bus test system can be found in Ref. [40]. The maximum active power output and maximum spinning reserve of the slack bus are 4 MW and 1 MV, respectively. The power capability limit of the BESS unit is 100 kVA. The maximum and minimum SOC of the BESS unit are 200 and 1000 kVh, respectively. The initial percentage of SOC for BESS is 25% [32]. The locations of MMGs and BESSs are determined by active participation factors (APFs) [41]. In Fig. 4, the seven most critical buses due to the high level of APFs are illustrated in bold. The penalty price is set to 0.5 $/kWh, and the regulation market prices are the same as that shown in Table 3. In the subsequent cases, the peak load is obtained from Ref. [40] and the remaining daily load profile follows a typical load curve from the California Independent System Operator (CAISO) [42], as shown in Fig. 7.

Table 4
Pareto optimal solution of the deterministic case for the MMG system.

#	W_1	W_2	J_1 ($)	J_2 (pu)	$J_{1,pu} = \frac{J_{1,\max} - J_1}{J_{1,\max} - J_{1,\min}}$	$J_{2,pu} = \frac{J_{2,\max} - J_2}{J_{2,\max} - J_{2,\min}}$	$\min(J_1, J_2)$
1	1.0	0.0	302.83630	13.45220	1	0	0
2	0.9	0.1	310.83630	11.95038	0.99270	0.11164	0.11164
3	0.8	0.2	330.83630	10.45038	0.97446	0.22315	0.22315
4	0.7	0.3	350.84291	8.94227	0.95622	0.33526	0.33526
5	0.6	0.4	370.92421	7.86899	0.93791	0.41504	0.41504
6	0.5	0.5	403.10509	6.26032	0.90856	0.53462	0.53462
7	**0.4**	**0.6**	**503.49378**	**3.96092**	**0.81700**	**0.70556**	**0.70556**
8	0.3	0.7	634.72534	2.79051	0.69732	0.79256	0.69732
9	0.2	0.8	811.94606	1.68838	0.53570	0.87449	0.53570
10	0.1	0.9	1053.38685	0.89939	0.31551	0.93314	0.31551
11	0.0	1.0	1399.35007	0.00000	0	1	0

The highlighted row (in bold font) corresponds to the best compromise Pareto optimal solution.

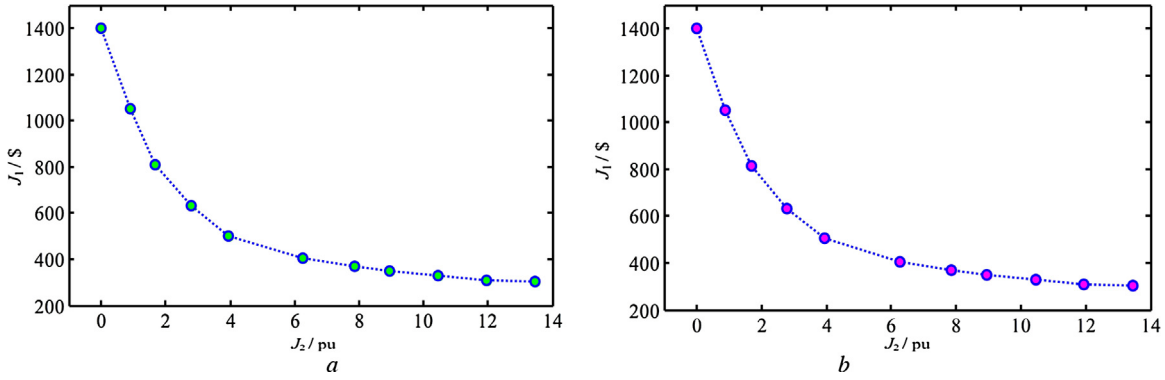

Fig. 8. Pareto front of the MMG test case: (a) Scenario I and (b) Scenario II.

5.2. Results and analysis of the DPICP model

The results of three different scenarios are compared to illustrate the effectiveness of the proposed method clearly (T is set to 24 h and starting time k is set to 0):

(I) Deterministic optimization;
(II) Uncertainty characterization using the PEM;
(III) Uncertainty characterization using the MC.

In Scenario I, only the mean value of the random variables for 24 h is considered in the DPICP model. The calculated maximum and minimum values of the MMG operation cost (J_1) are $1399.35007 and $302.83630, respectively, and the calculated maximum and minimum values of power interchange robustness (J_2) are 13.45220 and 0.00000 pu, respectively. These values are used to solve the multi-objective function expressed in Eq. (1). These border values are obtained by maximizing and minimizing the objective functions of the DPICP model individually.

Table 4 shows the values of the objective functions for all 11 Pareto optimal solutions. The fuzzy satisfying method is utilized in this study to select the best solution among the obtained Pareto optimal sets. The last column of Table 4 clearly indicates that the optimal solution is #7, with the maximum weakest membership function of 0.70556. The corresponding MMG operation cost and power interchange robustness are equal to $503.49378 and 3.96092 pu, respectively. Correspondingly, the Pareto optimal front of the objective functions is calculated as depicted in Fig. 8a.

In Scenario II, the stochastic behaviors of the PV, the WT power, the electricity load, and the heat load are considered. In this section, PEM is employed to model the uncertainties with respect to its mean and STD values. In this scenario, the expected MMG operation cost is higher than that of the deterministic scenario. The mean values of the objective functions are also summarized in Table 5. As shown in Table 5, solution #7 is the optimal solution. The Pareto optimal front of the objective functions is derived as depicted in Fig. 8b.

From the results of Scenarios I and II, the Pareto optimal solutions for the DPICP model are derived, as shown in Fig. 9a and b. In this study, the weighting factors are determined by the fuzzy satisfying method, and the Pareto optimal solution is regarded as the PICs uploaded to the DNCC. Fig. 9c and d illustrates the range of PICs at the 6th, 12th, and 18th hours. These figures show that the upper limit of the PICs exceeds the transmission capacity limit (100 kW) at the 12th and 18th hours.

The MC method was used to obtain the results of the DPICP model in Scenario III to verify the accuracy of Hong's PEM ($2m+1$ scheme). The results of MC are reported for 10,000 trial simulations. Table 6 shows the individual maximum relative errors of the first seven moments of the power interchange capability limits. The individual relative error for the r-order moment of the upper and lower limits of the power interchange capability in the PEM for the jth microgrid at hour t, that is, $\varepsilon_{\mu^r P_{PCC}^{j,t,up/dn}}$, is expressed in following equations [27]. The values in Table 6 show the high level of accuracy of the results for all moments.

$$\varepsilon_{\mu^r P_{PCC}^{j,t\,up/dn}} = 100 \cdot \frac{|\mu^{r,PEM}_{P_{PCC}^{j,t,up/dn}} - \mu^{r,MC}_{P_{PCC}^{j,t,up/dn}}|}{P_{PCC}^{j,\max}} \tag{51}$$

$$\varepsilon_{\mu^r P_{PCC}^{\max}} = \max_{j,t}\{\varepsilon_{\mu^r P_{PCC}^{j,t,up/dn}}\} \quad j = 1, 2, \quad t = k+1, \ldots, k+T \tag{52}$$

5.3. Results and analysis of the DPICC model

The PICs of MG3, MG4, and MG6 are assumed equal to MG2, and the PICs of MG5 and MG7 are assumed equal to MG1 to simulate the condition of seven grid-connected microgrids operating in the 33-bus test distribution system, as shown in Fig. 4. Then, the PICs,

Table 5
Pareto optimal solution of the PEM for the MMG system.

#	W_1	W_2	J_1 ($)	J_2 (pu)	$J_{1,pu} = \frac{J_{1,\max} - J_1}{J_{1,\max} - J_{1,\min}}$	$J_{2,pu} = \frac{J_{2,\max} - J_2}{J_{2,\max} - J_{2,\min}}$	min (J_1, J_2)
1	1.0	0.0	303.07711	13.45118	1	0	0
2	0.9	0.1	310.95490	11.95102	0.99260	0.11159	0.11159
3	0.8	0.2	330.84769	10.44568	0.97445	0.22350	0.22350
4	0.7	0.3	350.95416	8.94053	0.95612	0.33538	0.33538
5	0.6	0.4	371.22965	7.86916	0.93763	0.41503	0.41503
6	0.5	0.5	403.12370	6.25972	0.90854	0.53467	0.53467
7	**0.4**	**0.6**	**503.50980**	**3.95988**	**0.81699**	**0.70563**	**0.70563**
8	0.3	0.7	634.82886	2.79008	0.69723	0.79259	0.69723
9	0.2	0.8	812.26453	1.68797	0.53541	0.87452	0.53541
10	0.1	0.9	1054.18504	0.89923	0.31478	0.93315	0.31478
11	0.0	1.0	1400.65705	0.00000	0	1	0

The highlighted row (in bold font) corresponds to the best compromise Pareto optimal solution.

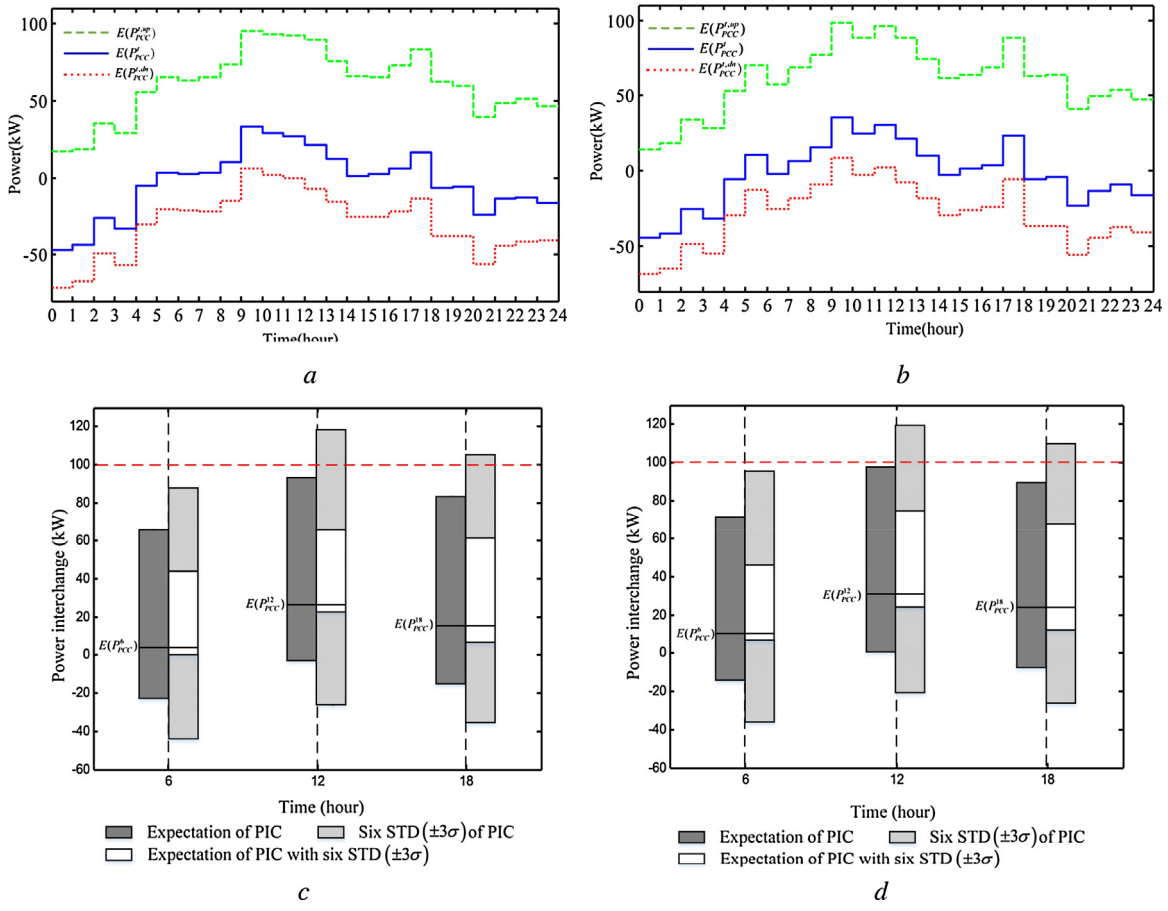

Fig. 9. Power interchange capabilities: (a) mean value of the power interchange limits for MG1, (b) mean value of the power interchange limits for MG2, (c) PICs for MG1 considering STD, and (d) PICs for MG2 considering STD.

Table 6
Individual maximum relative errors of the first seven moments of the power interchange capabilities.

r-order moment	1st	2nd	3rd	4th	5th	6th	7th
Individual maximum relative error (%)	0.669	0.832	0.932	1.146	1.108	0.770	1.005

including the power transactions, of all microgrids are uploaded to the DNCC. Fig. 10 displays the AICs of MG1 and MG2 calculated by the DNCC using the SOCP with varied spinning reserve requirements. The calculations show that the higher the spinning reserve requirement, the more the interchange power capacity is corrected. As shown in Fig. 10, the distribution system experiences up spinning reserve shortage at the period of 14:00–21:00 because the DN load demand reaches its peak value at this period as well as the spinning reserve requirement. Only the AICs for the first hour report to the MGCCs under the MPC-based scheme.

The SQP-based method [43] is selected and compared with the SOCP-based method to verify the effectiveness of the proposed method, and the total amounts of corrected ramping capabilities and the DN operation costs are shown in Table 7. The SOCP formulation provides better operating points than the SQP formulation.

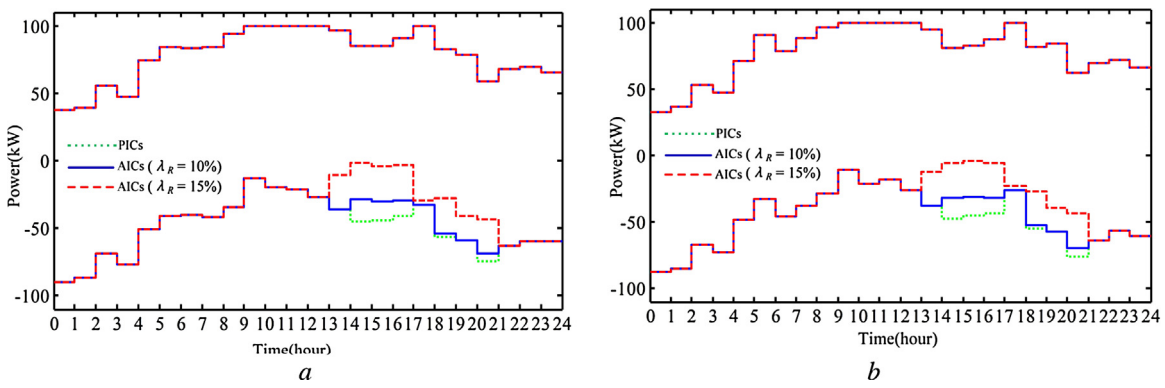

Fig. 10. PICs and AICs with λ_R = 10% and λ_R = 15%: (a) MG1 and (b) MG2.

Table 7
Results from the SQP and SOCP formulations of the DPICC model with varied spinning reserve requirements.

Rate of spinning reserve		λ_R = 6%	λ_R = 7%	λ_R = 8%	λ_R = 9%	λ_R = 10%
Total corrected ramping capabilities (kWh)	SQP [43]	0	2.94695	67.43812	185.75744	350.40264
	SOCP	0	2.94668	67.43107	185.72750	350.34630
$F_2(\boldsymbol{X}_2)$ ($)	SQP [43]	6457.01022	6460.14619	6491.74501	6549.64502	6631.85390
	SOCP	6456.32458	6457.79792	6490.04012	6549.18834	6631.49774

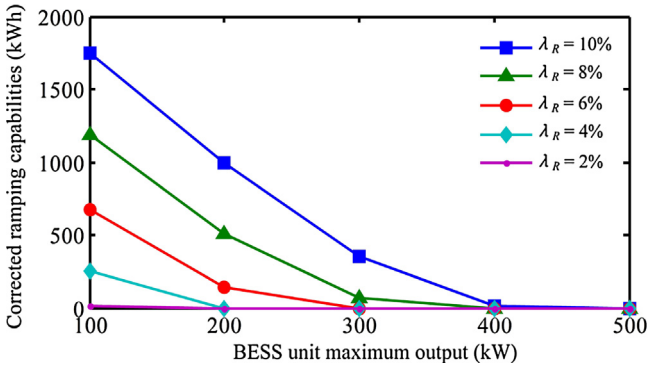

Fig. 11. Spinning reserve requirement and the corrected ramping capability variation with the BESS unit maximum output.

Table 8
Results of DN operation cost and power loss with varied BESS unit capacities (λ_R = 6%).

Maximum SOC of the BESS unit (kWh)	500	1000	1500	2000
$F_2(\boldsymbol{X}_2)$ ($)	6510.21	6456.32	6419.94	6402.08
Power loss (kWh)	2521.34	2516.13	2500.28	2500.07

This test case considers the variations of the BESS unit maximum output from 100 kW to 500 kW and the spinning reserve requirement from 2% to 10% to analyze the sensitivity of the BESS unit's maximum output and total corrected capabilities. Fig. 11 shows that as the BESS unit's maximum output increases, the corrected capabilities decrease. When the BESS unit's maximum output is greater than 400 kW and the spinning reserve requirement is less than 10%, no corrective capabilities are observed because of the sufficient reserve space supplemented by the BESS.

In addition to providing spinning reserve, the energy pool of the BESS is used to reduce the generation cost and alleviate line congestion. As shown in Table 8, the DN operation cost and power loss decrease as the BESS unit's maximum SOC increases. On one hand, the BESS is used to store energy during the off-peak period and discharge power at peak times to reduce the operation cost. On the other hand, the BESS provides the DNCC with active and reactive powers to alleviate line congestion and decrease the power loss.

6. Conclusion

The increasing frequency and growing capacity of power interchange between MMGs and DN are expected to affect the operational aspects of power systems. Given that microgrids may be independent systems with different rules, constraints, and objectives, the secure ranges for dynamic interchange adjustments must be estimated. This study proposes a new modeling framework that consists of the DPICP and DPICC models. Each independent microgrid can accomplish its own set of objectives with AICs.

The proposed methodology is tested on a 33-bus distribution system with MMGs. The high accuracy of the proposed PEM-based method is verified through comparisons with the MC method. The integration of large BESS (with a maximum output of up to 400 kW) is permissible for the 10% spinning reserve requirement without PICs to be corrected. Furthermore, the results of the proposed model can enhance situation awareness and assist microgrids in participating in the ramp and demand response markets.

The proposed framework can be easily extended to other microgrid and distribution system operation applications. Specifically, the objective function of the DPICP model can be modified to satisfy different microgrid operation modes. The DPICC model can be applied to other distribution systems that are integrated with wind farms and PV systems to ensure secure operations on the DN level.

Acknowledgments

This research is partly supported by the National Natural Science Foundation of China (no. 51577115) and the National High Technology Research and Development Program of China (2016YFB0901304).

Appendix A. Supplementary data

Supplementary data associated with this article can be found, in the online version, at http://dx.doi.org/10.1016/j.epsr.2017.07.001.

References

[1] F. Katiraei, R. Iravani, N. Hatziargyriou, A. Dimeas, Microgrids management, IEEE Power Energy Mag. 6 (2008) 54–65.

[2] R. Lassetter, A. Akhil, C. Marnay, Integration of Distributed Energy Resources: The CERTS Microgrid Concept. CERT Report, Office of Scientific & Technical Information Technical Reports, 2002.
[3] N. Hatziargyriou, Operation of Multi-microgrids, first ed., Wiley-IEEE Press, 2014.
[4] R.H. Lasseter, Smart distribution: coupled microgrids, Proc. IEEE 99 (2011) 1074–1082.
[5] A. Kargarian, M. Rahmani, Multi-microgrid energy systems operation incorporating distribution-interline power flow controller, Electr. Power Syst. Res. 129 (2015) 208–216.
[6] N. Nikmehr, S.N. Ravadanegh, Optimal power dispatch of multi-microgrids at future smart distribution grids, IEEE Trans. Smart Grid 6 (2015) 1648–1657.
[7] J. Wu, X. Guan, Coordinated multi-microgrids optimal control algorithm for smart distribution management system, IEEE Trans. Smart Grid 4 (2013) 2174–2181.
[8] M.A. Bucher, S. Chatzivasileiadis, G. Andersson, Managing flexibility in multi-area power systems, IEEE Trans. Power Syst. 31 (2016) 1218–1226.
[9] C. Wan, J. Lin, W. Guo, Y. Song, Maximum uncertainty boundary of volatile distributed generation in active distribution network, IEEE Trans. Smart Grid 1 (2016) 1–13.
[10] W. Wei, F. Liu, S. Mei, Dispatchable region of the variable wind generation, IEEE Trans. Power Syst. 30 (2015) 2755–2765.
[11] Dobson, Computing a closest bifurcation instability in multidimensional parameter space, J. Nonlinear Sci. 3 (1993) 307–327.
[12] H.D. Chiang, A.J. Flueck, K.S. Shah, N. Balu, CPFLOW: a practical tool for tracing power system steady-state stationary behavior due to load and generation variations, IEEE Trans. Power Syst. 10 (1995) 623–634.
[13] C. Cañizares, A. Claudio, C.L. Demarco, I. Dobson, W.F. Long, Point of collapse methods applied to AC/DC power systems, IEEE Trans. Power Syst. 7 (1992) 673–683.
[14] V. Ajjarapu, C. Christy, The continuation power flow: a tool for steady state voltage stability analysis, IEEE Trans. Power Syst. 7 (1992) 416–423.
[15] G.D. Irisarri, X. Wang, J. Tong, S. Mokhtari, Maximum loadability of power systems using interior point nonlinear optimization method, IEEE Trans. Power Syst. 12 (1997) 162–172.
[16] J.C.O. Mello, A.C.G. Melo, S. Granville, Simultaneous transfer capability assessment by combining interior point methods and Monte Carlo simulation, IEEE Trans. Power Syst. 12 (1997) 736–742.
[17] J.H. Liu, C.C. Chu, Iterative distributed algorithms for real-time available transfer capability assessment of multi-area power systems, IEEE Trans. Smart Grid 6 (2015) 2569–2578.
[18] X. Zhang, S. Grijalva, Decentralized total transfer capability evaluation using domain decomposition methods, IEEE Trans. Power Syst. 31 (2016) 3349–3357.
[19] C. Wu, G. Hug, S. Kar, Risk-limiting economic dispatch for electricity markets with flexible ramping products, IEEE Trans. Power Syst. 31 (2016) 1990–2003.
[20] A. Pina, C.A. Silva, P. Ferrão, High-resolution modeling framework for planning electricity systems with high penetration of renewables, Appl. Energy 112 (2013) 215–223.
[21] J. Zhao, T. Zheng, E. Litvinov, A unified framework for defining and measuring flexibility in power system, IEEE Trans. Power Syst. 31 (2015) 339–347.
[22] S.M. Mohseni-Bonab, A. Rabiee, B. Mohammadi-Ivatloo, S. Jalilzadeh, A two-point estimate method for uncertainty modeling in multi-objective optimal reactive power dispatch problem, Int. J. Electr. Power Energy Syst. 75 (2015) 194–204.
[23] S. Chen, H.B. Gooi, M.Q. Wang, Sizing of energy storage for microgrids, IEEE Trans. Smart Grid 3 (2012) 142–151.
[24] A.K. Basu, A. Bhattacharya, S. Chowdhury, S.P. Chowdhury, Planned scheduling for economic power sharing in a CHP-based micro-grid, IEEE Trans. Power Syst. 27 (2012) 30–38.
[25] H. Farzin, M. Fotuhi-Firuzabad, M. Moeini-Aghtaie, Enhancing power system resilience through hierarchical outage management in multi-microgrids, IEEE Trans. Smart Grid 7 (2016) 2869–2879.
[26] M. Marinelli, F. Sossan, G.T. Costanzo, H.W. Bindner, Testing of a predictive control strategy for balancing renewable sources in a microgrid, IEEE Trans. Sustainable Energy 5 (2014) 1426–1433.
[27] F.J. Ruiz-Rodriguez, J.C. Hernandez, F. Jurado, Voltage unbalance assessment in secondary radial distribution networks with single-phase photovoltaic systems, Int. J. Electr. Power Energy Syst. 64 (2015) 646–654.
[28] P. Li, Z. Zhou, R. Shi, Probabilistic optimal operation management of microgrid using point estimate method and improved bat algorithm, in: IEEE Power and Energy Society General Meeting, Washington, DC, 2014.
[29] C.L. Su, Probabilistic load-flow computation using point estimate method, IEEE Trans. Power Syst. 20 (2005) 1843–1851.
[30] H. Lee Willis, Power Distribution Planning Reference Book, CRC Press, 2004.
[31] M.M.A. Abdelaziz, H.E. Farag, E.F. El-Saadany, A.R.I. Mohamed, A novel and generalized three-phase power flow algorithm for islanded microgrids using a newton trust region method, IEEE Trans. Power Syst. 28 (2013) 190–201.
[32] M. Qin, K.W. Chan, Y.C. Chi, X. Luo, Optimal planning and operation of energy storage systems in radial networks for wind power integration with reserve support, IET Gener. Transm. Distrib. 10 (2016) 2019–2025.
[33] W. Mai, C.Y. Chung, Economic MPC of aggregating commercial buildings for providing flexible power reserve, IEEE Trans. Power Syst. 30 (2014) 1–10.
[34] J.M. Morales, J. Pérez-Ruiz, Point estimate schemes to solve the probabilistic power flow, IEEE Trans. Power Syst. 22 (2007) 1594–1961.
[35] P. Caramia, G. Carpinelli, P. Varilone, Point estimate schemes for probabilistic three-phase load flow, Electr. Power Syst. Res. 80 (2010) 168–175.
[36] A. Baziar, A. Kavousi-Fard, Considering uncertainty in the optimal energy management of renewable micro-grids including storage devices, Renew. Energy 59 (2013) 158–166.
[37] K.V. Mardia, J.T. Kent, J.M. Bibby, Multivariante Analysis, Academic Press, London, 1997.
[38] M. Farivar, S.H. Low, Branch flow model: relaxations and convexification—part I, IEEE Trans. Power Syst. 28 (2013) 2554–2564.
[39] J.A. Taylor, F.S. Hover, Conic ac transmission system planning, IEEE Trans. Power Syst. 28 (2013) 952–959.
[40] J.Z. Zhu, Optimal reconfiguration of electrical distribution network using the refined genetic algorithm, Electr. Power Syst. Res. 62 (2002) 37–42.
[41] I. Kopcak, Silva L.C.P.D, V.F.D. Costa, J.S. Naturesa, Transmission systems congestion management by using modal participation factors, in: Power Tech Conference Proceedings, Bologna, 2003.
[42] J. Detmers, CAISO Operational Needs from Demand Response Resources, CAISO, 2012, Available at http://www.caiso.com/Documents.
[43] A.D.T. Le, M.A. Kashem, M. Negnevitsky, G. Ledwich, Optimal distributed generation parameters for reducing losses with economic consideration, in: Power Engineering Society General Meeting, Tampa, FL, 2007.